IEEE Robotics and Automation Letters (RAL) paper presented at the
2020 IEEE/RSJ International Conference on Intelligent Robots and Systems (IROS)
October 25-29, 2020, Las Vegas, NV, USA (Virtual)

Pneumatic Duplex-Chambered Inchworm Mechanism for Narrow Pipes Driven by Only Two Air Supply Lines

Tomonari Yamamoto[1], Sayako Sakama[1], Akiya Kamimura[1]

***Abstract*— Small in-pipe robots are key to improving pipe inspection procedures, especially for narrow diameters. However, robotic locomotion in such spaces, namely achieving a high locomotion performance with a narrow and flexible mechanism, is difficult. The novel in-pipe locomotion mechanism proposed in this paper achieves rapid locomotion through narrow pipes by a unique duplex-chambered structure. The mechanism achieves smooth bi-directional inchworm locomotion by a combination of expandable silicone rubber and a coil spring and is fully controlled by only two air supply lines. The concept and locomotion technique, including a mathematical analysis and discussion from the viewpoint of operational pressure, are presented herein. Several experiments on the prototyped mechanism were performed to elucidate its characteristics. The results of locomotion tests through horizontal, vertical, and bent pipes showed that the mechanism can horizontally navigate through 25-mm pipes at 45.5 mm/s, which is the fastest yet reported for this size of bi-directional in-pipe robot.**

I. Introduction

Pipe inspection is an important task that has long been a research focus in robotics. Pipes are essential industrial facilities that require periodic inner inspection for maintenance, but are often installed in locations with limited access, such as underground or inside walls. Normal endoscopic cameras, the current mainstream equipment for pipe inspection, are particularly insufficient for narrow pipes because their small inner space and complicated geometries limit the insertable area. In-pipe robots with small propulsion mechanisms are one solution to these issues. The development of in-pipe propulsion techniques will simplify inspection procedures and expand inspection areas.

Previous robots developed for narrow pipes with inner diameters of approximately 50 mm or less can be classified into two general groups: motor-driven and pneumatic-driven. Motor-driven mechanisms typically generate a driving force using wheels [1]–[5] or crawlers [6]–[9]. There are also snake-motion mechanisms driven by electric motors [10]–[13]. Motor-driven mechanisms have the overall advantages of a high driving force and locomotion speed. However, they are often difficult to apply to narrow or bending pipes because their mechanisms consist of rigid components, which are difficult to downsize.

Pneumatic-driven mechanisms are another approach to achieving smooth locomotion in narrow pipes. Peristaltic motion, a common mode of locomotion for robots with pneumatic mechanisms, generates earthworm-like motion using multiple air chambers [14]–[17]. One variation on peristaltic-motion mechanisms can generate one-directional locomotion using only one air supply tube [18]. Inchworm motion is also common for the locomotion of various robots [19]–[27], which generally involves three or more air chambers that are pressurized independently. There are also small inchworm mechanisms that can move in only one direction but are driven by a single air supply tube [28], [29]. Other unique pneumatic mechanisms include helical motion [30], [31] and sliding-inchworm motion, which was previously developed by the authors [32]–[34]. Pneumatic-driven robots are advantageous for narrow or bending pipes because of their simplicity and flexibility; they are also explosion-proof in a flammable working environment. However, their locomotion speed is generally low compared with that of motor-driven robots, and they require many air supply tubes for bi-directional locomotion.

Figure 1 compares the speeds of pneumatic robots according to their applicable diameter. Many have a speed less than 30 mm/s and applicable diameter less than 60 mm. The two fastest robots cannot move backward [28], [29], while the next fastest moves at 45.0 mm/s in 20-mm pipes but slows to 10.0 mm/s in 25-mm pipes. This comparison suggests a robot capable of steady high-speed bi-directional locomotion through narrow pipes as the next target.

Locomotion in narrow pipes is challenging for robots because of the unique geometrical environment. The mechanisms must satisfy multiple requirements as summarized below, including significant limitations to body size and structure, to navigate through narrow pipes.

- **Narrow body diameter**: The mechanism must have a narrow enough body to pass through the pipes. Mechanism simplicity is also preferable for downsizing.
- **Flexible body structure**: The mechanism must be bendable to pass through bending pipes.
- **Bi-directional locomotion**: The robot must be able to move both forward and backward to exit the pipes.

The following capabilities are also preferable for improving the robot usefulness:

- **Fast locomotion**: More rapid locomotion would reduce inspection times.
- **Fewer, lighter tethers**: The robot must be wired as a lifeline for removal in case of failure. Air supply tubes can act as tethers and should be few in number to reduce their weight and required traction force.
- **Electric device-less mechanism**: Robots passing through pipes used for flammable gas or liquid must be explosion-proof. An electric-less mechanism is ideal for such environments.

In this study, we designed a novel pneumatic mechanism for narrow pipes that we named the pneumatic duplex-

This work was supported by JSPS KAKENHI Grant Number JP19K23502.

[1]The authors are with the National Institute of Advanced Industrial Science and Technology (AIST), Tsukuba, Japan {yamamoto.t, s-sakama, kamimura.a}@aist.go.jp

This paper has supplementary downloadable material provided by the authors. The enclosed video file includes an overview of the mechanism structure and locomotion pattern as well as footage of an in-pipe locomotion test.

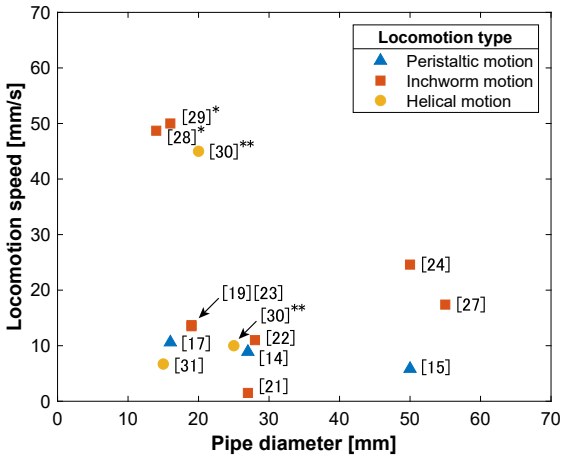

Fig. 1. Comparison of locomotion speed of pneumatic robots. Note that [28]* and [29]* have only one-directional locomotion, and the speed of [30]** differs greatly depending on the pipe diameter.

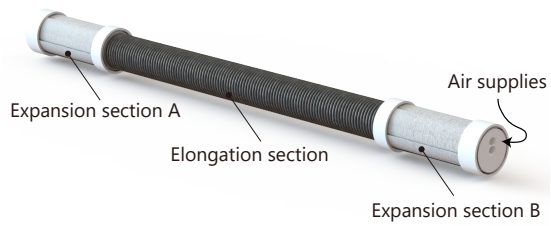

Fig. 2. Conceptual outer 3d-image of P-DCI mechanism.

chambered inchworm (P-DCI) mechanism. The P-DCI mechanism has unique dual-layered flexible chambers for high-speed bi-directional inchworm motion requiring only two air supply lines. Herein, we present the mechanical design of the P-DCI mechanism and evaluate its basic characteristics through modeling and experiments, including in-pipe trials with a prototyped mechanism through 25-mm pipes.

II. Design and Locomotion Technique

A. Structure and working principle

Figures 2 and 3 show the exterior and interior structure, respectively, of the P-DCI mechanism. The mechanism has two chambers made from silicone rubber, chambers A and B, that are partially overlapped. The mechanism is divided into three functional sections: expansion sections A and B and the elongation section.

Expansion sections A and B on the mechanism ends consist of single layers of chambers A and B, respectively. The outside of the expansion sections is covered by pleated fabric, allowing for radial chamber expansion but restricting axial extension.

The elongation section in the center of the mechanism is where chambers A and B overlap, i.e., chamber A is surrounded by chamber B. Thus, airflow into chamber A passes into both expansion section A and the outer layer of the elongation section; similarly, airflow into chamber B passes into both expansion section B and the inner layer of the elongation section. The outside of chamber A in the elongation section is covered by a coil spring, allowing for axial chamber extension but restricting radial expansion.

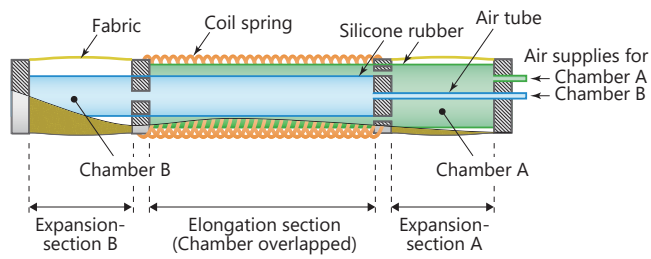

Fig. 3. Illustration representing interior structure of P-DCI mechanism.

B. Locomotion generation

Figure 4 shows the basic pattern for forward locomotion of the P-DCI mechanism. P_A and P_B are defined as the pressures in chambers A and B, respectively. P_0 is the initial pressure with no applied air, and P_1, P_2, P_3, and P_4 are the operating pressures applied to the mechanism, which satisfy

$$P_0 < P_1 < P_2 < P_3 \leq P_4. \tag{1}$$

Step 0 is the initial mechanism condition, i.e., no applied air. Locomotion is achieved by repeating steps 1 to 7 in order as follows:

Step 1: Pressurization of chamber A to P_1. Expansion section A inflates radially and grips the pipe wall. The elongation section does not yet extend.

Step 2: Pressurization of chamber A to P_3. By increasing P_A A from P_1 to P_3, the elongation section extends in the axial forward direction.

Step 3: Pressurization of chamber B to P_4. Expansion section B inflates radially. Chamber B in the elongation section also expands to occupy the elongation chamber A space because $P_3 \leq P_4$.

Step 4: De-pressurization of chamber A to P_0. Expansion section A shrinks and separates from the pipe wall. The elongation section remains extended because chamber B expanded into the spring in Step 3.

Step 5: De-pressurization of chamber B to P_2 shrinks the elongation section. Because expansion section B is still inflated, the elongation section shrinks in the forward direction.

Step 6: Pressurization of chamber A to P_1. Expansion section A expands and grips the pipe wall.

Step 7: De-pressurization of chamber B to P_0. Expansion section B shrinks and separates from the pipe wall, reverting the state of the mechanism to Step 1.

Note that either expansion section A or B must grip the pipe wall at all times to avoid moving in unintended directions in horizontal pipes or falling in vertical pipes.

Now, we consider the applied pressures conditions to invoke the above motion pattern. Let P_{exA}, P_{exB}, and P_{el} represent the threshold pressures to activate expansion sections A and B and the elongation section, respectively. We assume P_{exA} and P_{exB} satisfy

$$P_{exA} \leq P_{exB} < P_{el}. \tag{2}$$

The pressure condition to trigger STEP 1 can be written as

$$P_{exA} \leq P_1 < P_{el}. \tag{3}$$

Likewise, the condition for P_3 in STEP 2 can be written as

$$P_{el} \leq P_3. \tag{4}$$

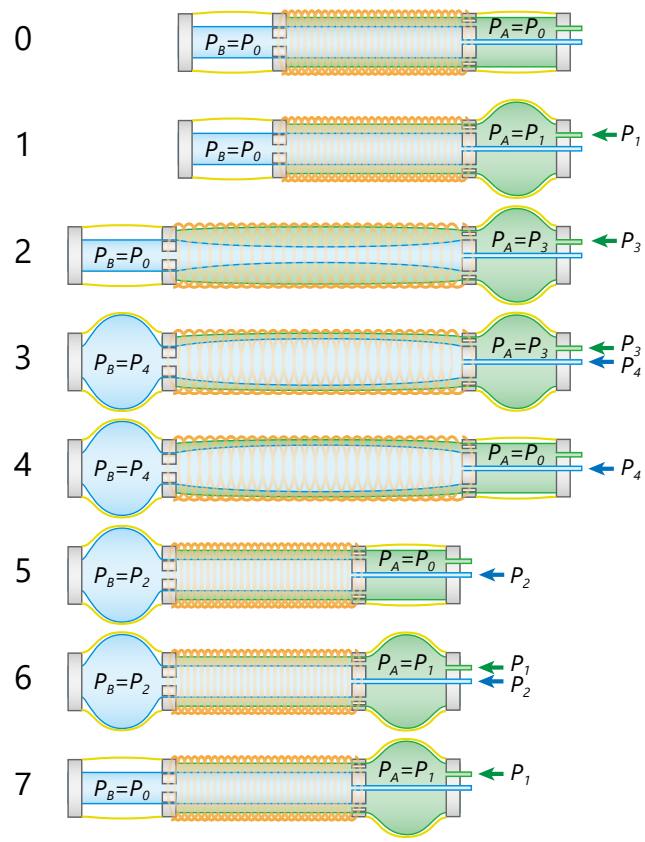

Fig. 4. Pattern for forward locomotion. The numbers on the left indicate the steps.

In Step 3, P_4 must be higher than P_3 because the volume of chamber B in the elongation section is pressurized by chamber A in Step 3. This can be expressed by

$$P_{el} \leq P_4, \tag{5}$$

$$P_3 \leq P_4. \tag{6}$$

Then, in Step 5, P_2 must satisfy

$$P_{exB} \leq P_2 < P_{el}. \tag{7}$$

From these inequalities, the pressure conditions for locomotion can be expressed as

$$P_0 < P_{exA} \leq P_1 < P_{exB} \leq P_2 < P_{el} \leq P_3 \leq P_4. \tag{8}$$

C. Theoretical analysis for expansion

P_{exA}, P_{exB}, and P_{el} are important for selectively activating the expansion and elongation sections. Thus, these thresholds should be estimated for prototyping. Here, we discuss these thresholds considering the expansion characteristics of silicon rubber and determine P_{exA} and P_{exB} by simulations.

Wakana et al. suggested a model for the relationship between the inflation and inner air pressure of an elastic rubber tube [35], which we adapted to our mechanism. According to their study, the relationship between P and R, the internal pressure and radius of the elastic tube, respectively, can be expressed as

$$P = \frac{R - R_0}{R^2}\left(\frac{Et_0}{1-\nu^2}\right), \tag{9}$$

TABLE I
PARAMETERS FOR P-DCI SIMULATION.

	Chamber A	Chamber B
R_{exX0} [mm]	5.0	3.0
t_{exX0} [mm]	2.0	2.0
E [kPa]	83	
ν [–]	0.49	

* Subscript X means A or B.

where R_0, t_0, E, and ν are the initial inner radius, initial thickness, Young's modulus, and Poisson's ratio of the elastic tube, respectively.

First, we consider chamber A of the P-DCI mechanism. We define the inner radius and thickness of chamber A as R_{exA} and t_{exA} for expansion section A and R_{elA} and t_{elA} for the elongation section, respectively. Then, Eq. (9) can be rewritten as

$$P_A = \frac{R_{exA} - R_{exA0}}{{R_{exA}}^2}\left(\frac{E \cdot t_{exA0}}{1-\nu^2}\right) \textit{and} \tag{10}$$

$$P_A = \frac{R_{elA} - R_{elA0}}{{R_{elA}}^2}\left(\frac{E \cdot t_{elA0}}{1-\nu^2}\right), \tag{11}$$

where R_{exA0}, R_{elA0}, t_{exA0}, and t_{elA0} are the initial radii and thicknesses, respectively.

Next, we consider chamber B. We define the inner radius and thickness of chamber B as R_{exB} and t_{exB} for expansion section B and R_{elB} and t_{elB} for the elongation section, respectively. The inflation of chamber B can be expressed as

$$P_B = \frac{R_{exB} - R_{exB0}}{{R_{exB}}^2}\left(\frac{E \cdot t_{exB0}}{1-\nu^2}\right), \tag{12}$$

where R_{exB0} and t_{exB0} are the initial values. The inflation of chamber B in the elongation section is slightly different from that of chamber A. The silicone rubber of chamber B initially inflates alone, but eventually contacts chamber A and inflates more in combination. Thus, the inflation of chamber B in the elongation section is expressed as

$$P_B = \begin{cases} \dfrac{R_{elB} - R_{elB0}}{{R_{elB}}^2}\left(\dfrac{E \cdot t_{elB0}}{1-\nu^2}\right) & (R_{elB} < R_{elA0}) \\ \dfrac{R_{elB} - R_{elB0}}{{R_{elB}}^2}\left(\dfrac{E \cdot t_{elB0}}{1-\nu^2}\right) & \\ \quad + \dfrac{R_{elA} - R_{elA0}}{{R_{elA}}^2}\left(\dfrac{E \cdot t_{elA0}}{1-\nu^2}\right) & (R_{elA0} \leq R_{elB}) \end{cases} \tag{13}$$

where R_{elB0} and t_{elB0} are the initial radius and thickness, respectively. Note that in this equation, we ignore viscoelasticity from the contact between chambers A and B.

Figure 5 shows the analysis results for the expansion sections of the chambers based on Eqs. (10) and (12). The parameters in Table I were set based on the prototype discussed in Section II-D. From the results, we determined the threshold pressures P_{exA} and P_{exB} as 11 and 18 kPa, respectively. Because it is difficult to determine P_{el} using only Eq. (11) or (13) since it is also affected by the spring characteristics and mechanical configuration of the elongation section, we determined P_{el} experimentally as detailed in Section III-B.

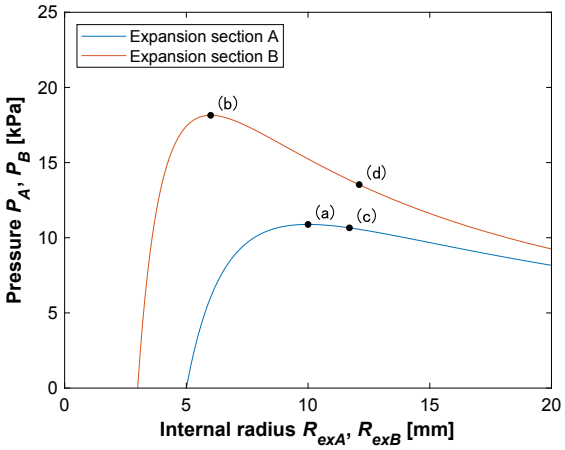

Fig. 5. Simulation results for expansion sections A and B. (a) and (b) indicate the minimum pressures for full inflation of chambers A and B, respectively, and (c) and (d) indicate the respective simulated radii at which the chambers contact the wall in a 25-mm pipe.

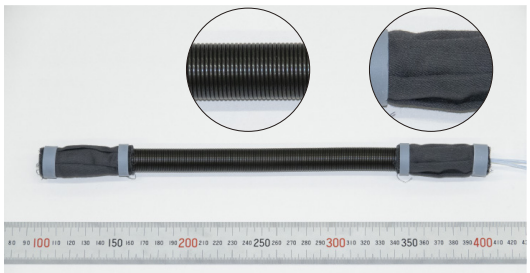

Fig. 6. Image of prototype P-DCI mechanism. Circular insets show partial enlargements of the elongation (left) and expansion sections (right).

TABLE II
SPECIFICATIONS OF THE P-DCI PROTOTYPE.

Item	Specification
Length	300 mm
(Expansion section)	45 mm
(Elongation section)	180 mm
Weight	97 g
Max outer dia.	22 mm

D. Prototyping

We constructed a prototype to embody the proposed concept, as shown in Fig. 6. The chambers were made from silicon rubber (EcoFlex 00-50, Smooth-On) by casting with 3d-printed molds. A coil spring with a spring coefficient of 0.04 N/mm was used, and the fabric covers around expansion sections A and B were pleated. A small initial inner radius is ideal to maintain a narrow robot body. In contrast, the body should be long to increase the elongation length. Here, these dimensions were determined by the accuracy and strength of the 3d-printed parts and maximum build size of the printer. The prototype specifications are listed in Table II.

III. EXPERIMENTS

Several experiments were conducted to analyze the characteristics and behavior of the proposed mechanism. All experiments were performed using the prototype with the same specifications.

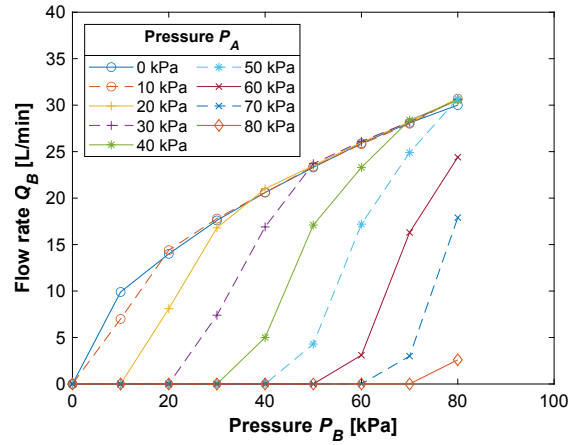

Fig. 7. Relationship between applied pressure and airflow through chamber B.

A. Pressure difference and airflow characteristics

The P-DCI mechanism uses pressure differences to generate motion as explained in Section II. Especially, the airflow characteristics of chamber B in Step 3 are interesting and unknown. Therefore, we measured the airflow into the expansion section of chamber B while chamber A was pressurized. The experiment was conducted as follows:

Method: The prototype was placed in a 25-mm-diameter pipe to maintain its straight shape. Operational air was applied into one end on the chamber A side. The chamber B side was open and connected to a flow sensor. We pressurized chambers A and B to several pressures and measured the flow rate out through the elongation section of chamber B.

Result: Figure 7 shows the experimental results illustrating how the flow rate of chamber B, Q_B, changed depending on P_A and P_B. Q_B increased non-linearly with increasing P_B and decreased with increasing P_A. Q_B is non-zero when P_B is equal to or higher than P_A.

The results indicate that the pressurization of chamber A causes chamber B to narrow, which stops the airflow. Thus, when the P-DCI mechanism moves using the motion pattern shown in Fig. 4, P_4 must be equal to or greater than P_3, as stated in Eq. (1).

B. Elongation length characteristics

We elucidated the elongation characteristics experimentally and determined P_{el}, the threshold pressure to activate the elongation section. The experiment was conducted as follows:

Method: The prototype was placed in a 25-mm-diameter pipe to maintain its straight shape. Expansion sections A and B were enclosed in rigid covers to prevent expansion. One end of the mechanism was fixed to the pipe. The elongation length was measured while chamber A or B was pressurized in the range of 0 to 100 kPa in 10-kPa steps. The elongation length was recorded during both pressurization and depressurization to examine the effects of hysteresis. The measurements were performed 3 times for each chamber.

Result: Figures 8a and 8b show the measurement results for each chamber. The elongation length was almost proportional to the increase in pressure. A non-linear tendency occurred when the elongation length was 0 to 30 mm or longer than 150 mm. The maximum elongation lengths were

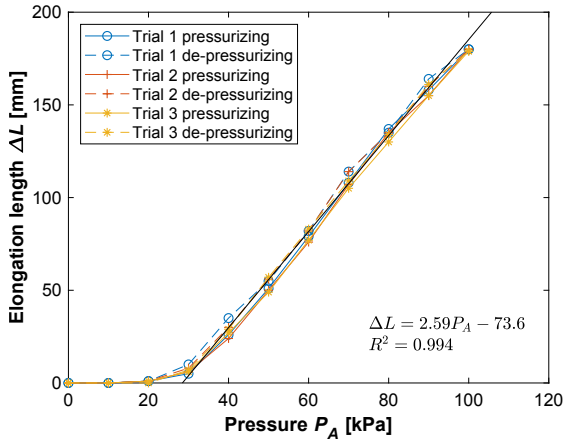

(a)

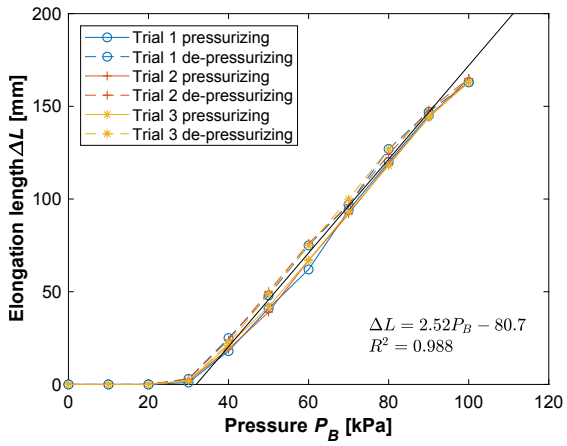

(b)

Fig. 8. Relationship between elongation length and applied pressure for chambers (a) A and (b) B.

180 and 165 mm for chamber A and B pressurization corresponding to elongation rates of 200% and 190%, respectively.

Slight hysteresis was observed, as the elongation lengths during de-pressurization were greater than those during pressurization. The maximum hysteresis difference was 5.6 mm for chamber A and 8.3 mm for chamber B. These can be considered sufficiently small compared with the elongation length.

The non-linear trend may mainly arise from the viscoelasticity of the silicone rubber. The tensile stress of rubber increases non-linearly with tensile strain, and its rate of increase is higher both when the rubber starts extending and when the extension approaches the fracture point. This may have affected the results of the experiment. The stress–strain trend of the prototype silicone rubber is unclear, which will require further examination in future work.

We approximated and linearly extrapolated the results for elongation lengths of 30 to 150 mm, as shown in black lines in Fig. 8a and 8b. The x intercepts, $P_A = 29$ kPa and $P_B = 32$ kPa, represent the minimum pressures to activate the respective elongation sections. Thus, we determined the threshold P_{el} as 32 kPa. Based on the discussions above and in Section II-C, the pressure conditions for locomotion can be expressed as

$$P_0 < 11 \leq P_1 < 18 \leq P_2 < 32 \leq P_3 \leq P_4 \text{ [kPa]}. \quad (14)$$

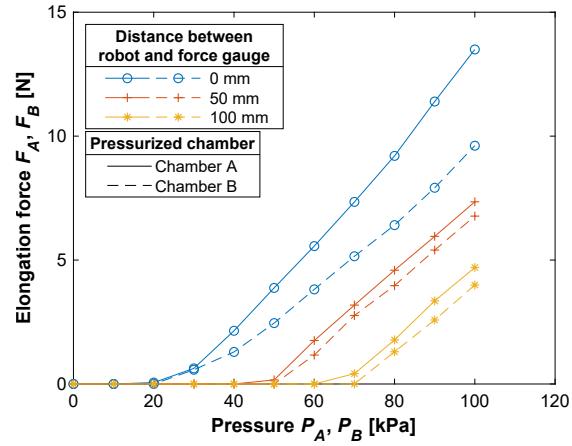

Fig. 9. Relationship between applied pressure and generated elongation force for chambers A and B.

C. Elongation force characteristics

We examined the elongation force when air was applied. In real operation, the mechanism will carry inspection equipment. Thus, the elongation force is important to evaluate. The elongation force was measured as follows:

Method: The prototype was placed in a 25-mm-diameter pipe to maintain its straight shape. Expansion sections A and B were enclosed in rigid covers to prevent expansion. One end of the mechanism was fixed to the pipe, while the other remained unfixed. A force gauge was attached to the free end and positioned at distances 0, 50, and 100 mm away, which correspond to the elongation length. The forces were recorded by the force gauge while chamber A or B was pressurized at 0 to 100 kPa in 10-kPa steps. The measurements were performed 3 times for each condition.

Result: Figure 9 shows the averaged results for each chamber. F_A and F_B, the elongation forces for chambers A and B, respectively, increased linearly with increasing pressure and decreased at greater distances between the mechanism and force gauge. The maximum forces of 13.5 and 9.6 N for chambers A and B, respectively, were recorded at a distance of 0 mm.

The results show that the elongation force is linearly dependent on applied pressure. The elongation force of an actuator consisting of a coil spring and chamber can be expressed as the product of the pressure and cross-sectional area [29]. Strictly speaking, the cross-sectional area of our P-DCI mechanism is not constant due to its two-layered structure and elasticity. Nevertheless, the results show that changes in the cross-sectional area do not greatly affect the elongation force.

The results also show that the elongation force is strongly correlated to the elongation length. When the elongation length was 100 mm, corresponding to an elongation rate of nearly 150%, the elongation forces decreased to 35% and 42% of the maximum for chambers A and B, respectively. This is due to tensile forces induced by the coil spring and chambers and suggests that the tensile force is non-linear.

The elongation force pushes the inspection equipment in front of the P-DCI mechanism, such as a camera or sensors, in Step 2 and thus determines the maximum load. For example, the maximum elongation force of chamber A, 13.5 N, is equivalent to the force required to push a 1.38-kg load

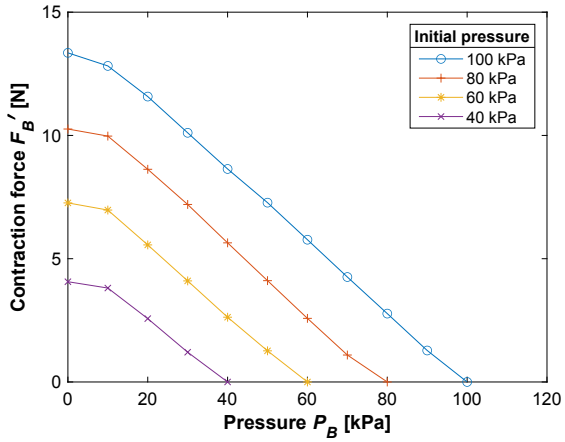

Fig. 10. Relationship between applied pressure and generated contraction force for chamber B.

in a vertical pipe. Although the actual pushing performance also depends on the friction between the load and pipes and the gripping performance of the expansion sections, it is enough for small inspection devices. For a heavy load, the applied pressure could be increased to increase the elongation force, or multiple P-DCI mechanisms could be attached together for one load.

D. Contraction force characteristics

We also examined the contraction force. The contraction force of chamber B in Step 5 is particularly important for estimating the locomotion distance. The contraction force was measured as follows:

Method: The prototype was placed in a 25-mm-diameter pipe to maintain its straight shape. The end of expansion section A was fixed to the pipe. Expansion section B was enclosed in a rigid cover to prevent expansion. Chamber B was pressurized to an initial pressure of 40, 60, 80, or 100 kPa, and a force gauge was attached. Then, the pulling force was recorded as chamber B was de-pressurized in 10-kPa steps. The measurements were performed 3 times for each condition.

Result: Figures 10 shows the averaged results. The contraction force for chamber B, $F_B{}'$, was linearly correlated to pressure P_B. The maximum force of 13.4 N was recorded at $P_B = 0$ kPa when the initial pressure was 100 kPa. The maximum force changed depending on the difference between the initial pressure and P_B, but no significant difference was observed in the rate of change.

The results show that the contraction force depends on the pressure difference between P_2 and P_4, as in Eq. (1), where a greater difference results in a higher contraction force. Considering the pressure conditions in Eq. (14), the contraction force of the prototype will be approximately 10 to 12 N if P_2 is 18 to 32 kPa and P_4 is 100 kPa. Thus, the mechanism can pull a load of 1.0 to 1.2 kg in vertical pipes if we assume no friction on the load and no slippage between the mechanism and pipes. Assuming the weight of a 4-mm-diameter tube is approximately 19 g/m, the mechanism can pull 27 to 32 m of two channels of tubes at a maximum. In practice, the locomotion distance will decrease because of friction between the air supply tubes and pipe wall. The traction also depends on the gripping performance of the expansion sections. The contraction force can be increased by increasing P_4, which could be realized using a coil spring with a higher spring coefficient. Multiple mechanisms for one robot could also increase the tractive load.

IV. In-pipe locomotion test

We tested the P-DCI mechanism in simulated pipes and observed its behavior. The recorded videos of each locomotion test are included in the supplemental material.

A. Locomotion test through straight pipes

Method: Horizontal pipes and vertical pipes with an inner diameter of 25 mm were used for the test. The P-DCI mechanism was inserted into the pipes, and air was applied for locomotion. The air was controlled by electro-pneumatic regulators and supplied via two air tubes 2.5 m in length with an inner diameter of 4 mm. The regulators were controlled by a sequence based on the locomotion pattern shown in Fig. 4. The applied pressures P_1, P_2, P_3, and P_4 were 30, 35, 80, and 100 kPa, respectively. Note that P_1 and P_2 were higher than the theoretical range shown in Eq. (14) because the regulators were unstable in such a low pressure range.

Result: Figures 11 and 12 show images captured while the mechanism was moving. Full locomotion videos are enclosed in the supplemental video material. The P-DCI mechanism worked well in both pipes and moved stably. The average speeds were 45.5 mm/s for horizontal locomotion, 23.7 mm/s for vertical climbing locomotion, and 54.4 mm/s for vertical descending locomotion. This horizontal locomotion speed is the highest compared with the other pneumatic in-pipe robots shown in Fig. 1. The averaged elongation lengths, which correspond to the locomotion distance per one cycle, were 142.5 mm for horizontal, 104.2 mm for vertical climbing, and 156.7 mm for vertical descending locomotion. The averaged horizontal elongation length corresponds to the experimental results shown in Fig. 8a.

There are two main reasons why vertical locomotion is slower while climbing: the weight of the air supply tubes acts in the opposite direction of locomotion, and the elongation section did not remain straight while extending because the body was too flexible to support its own weight while climbing. In contrast, while descending, the body remained straight and the weight of the tubes acted in the same direction as locomotion. Thus, descending was faster than climbing.

B. Locomotion test through bent pipes

Method: A total of eight types of 3d-printed bent pipes were used for the experiment. The bend angles were 45° and 90°, and the curvature radii were 25, 50, 80, and 110 mm; the pipes are shown in the supplemental video material. Each bent pipe was connected to straight pipes and placed horizontally. The other experimental conditions were the same as the previous tests.

Result: Figure 13 shows images captured while the mechanism was moving through the 90° bent pipe with a curvature of 50 mm. Videos of all the tests are included in the supplemental video material. The P-DCI mechanism successfully passed through the 45° pipes of all curvatures and the 90° pipes with 50-, 80-, and 110-mm curvatures. However, the mechanism could not pass through the 90° pipe with a curvature of 25 mm.

The results suggest that the capability of the mechanism to pass through a pipe bend depends on both the bend angle

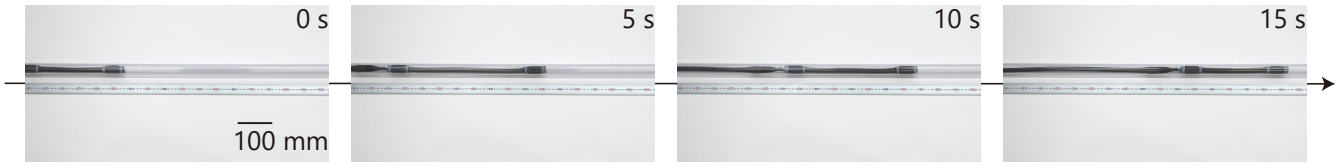

Fig. 11. Images captured in locomotion trial through 25-mm horizontal pipes.

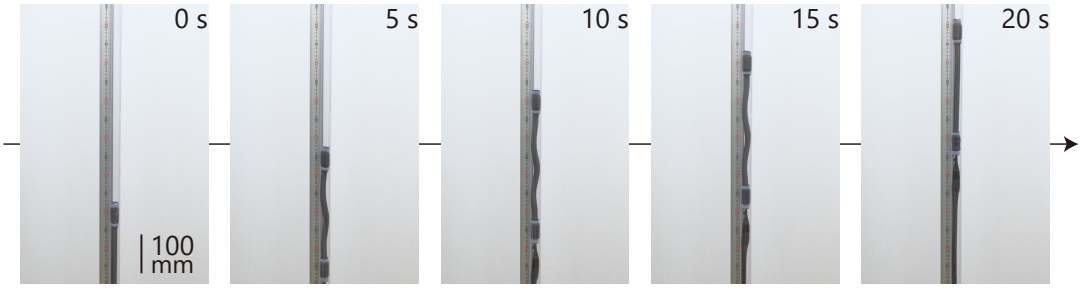

Fig. 12. Images captured in locomotion trial through 25-mm vertical pipes.

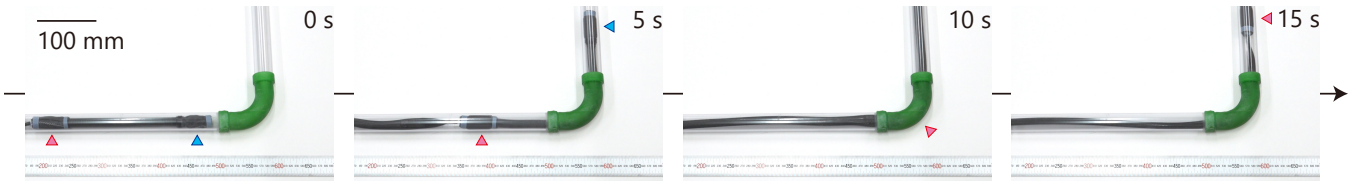

Fig. 13. Images captured in locomotion trial through a 90° pipe bend with a curvature of 50 mm. Blue and red triangles indicate the positions of chambers A and B, respectively.

and curvature. The 90° pipe with a 25-mm curvature that the P-DCI mechanism could not pass through was the most challenging experimental scenario. Failure occurred because the front of the P-DCI mechanism could not follow the steep curvature of the pipe wall, since the flexibility of chamber B caused it to easily bend upon colliding with the pipe wall. This could be improved by installing a guiding spring into chamber B to modify the flexibility. Additionally, the shape of the front of the P-DCI mechanism should also be improved for such steep pipe bends.

V. Discussion

The advantage of the P-DCI locomotion technique is that it can simultaneously satisfy all the requirements given in Section I. The unique duplex-chamber structure affords a narrow, flexible body with a simple structure, which lends itself toward further size reduction. Another structural benefit of the duplex chamber is that it does not require air tubes to be laid in the elongation section like other inchworm robots. This simplifies the tube layout inside the mechanism to easily obtained a high elongation rate. Furthermore, the mechanism is fully pneumatically driven, a significant advantage for operation in a flammable atmosphere.

One unique feature of the P-DCI mechanism is that it allows for bi-directional locomotion with only two air supply lines. More air supply tubes would increase the required tractive load and thereby greatly affect the locomotion distance. For example, if the tubes increased from 2 to 3, the required tractive force would increase by a factor of 1.5 and the locomotion distance would decrease to two-thirds. The locomotion style of the P-DCI mechanism lightens the tethers and decreases the required tractive load, which extends the locomotion distance. In addition, since the operational pressure is low, the mechanism can use thinner air tubes with a lower pressure resistance, which will also help make it lightweight.

The fast locomotion attributable to the long elongation distance and low tether weight is another remarkable characteristic of the P-DCI mechanism. The locomotion speed can be improved by increasing the elongation length per motion cycle, which can be achieved by simply raising P_3. A longer initial elongation section would also extend the elongation length during locomotion.

The speed can also be improved by reducing the time required for one motion cycle. The motion cycle period depends on the airflow rates, which are affected by the effective cross-sectional areas of the mechanism and air supply tubes. The effective cross-sectional area of the mechanism is mainly limited by the diameters of the intake ports and section dividers. Optimizing these designs to enlarge the cross-sectional area will increase the flow rates and decrease the motion cycle period. The effective cross-sectional area of the air supply tubes can be increased by enlarging their inner diameter. Since the P-DCI mechanism is driven by low air pressures, the diameter can be increased by reducing the tube thickness without increasing the tube outer diameter.

Another strategy to improve the locomotion speed is optimizing the valve control to increase the airflow rates. In this study, the applied air was regulated by constant pressure control for each locomotion step. This method is simple and steady but inefficient. An effective control method to increase the airflow rate would be to change the pressure

valve aperture considering not only the pressure but also the volume of applied air.

The locomotion performance, such as the speed and tractive load, is affected by the pipe wall conditions. Since the P-DCI mechanism grips the pipe wall by expanding each expansion section, its gripping force depends on the friction between the pipe wall and the fabric coverings. If the pipe wall is slippery due to water, oil, dust, etc., the locomotion speed and tractive force may decrease. The surface finish of the fabric on the expansion sections should be improved to obtain enough traction in such pipes.

Some other points must be improved to increase the performance and usefulness of the P-DCI mechanism. The structure should be modified to allow for easy camera installation, which could be realized with a hollow structure. The characteristics of the silicone rubber and coil spring should also be further investigated and optimized to obtain an increased traction force and speed. Other improvement points include a steering mechanism for branch pipes and air control techniques to drive multiple P-DCI mechanisms simultaneously and obtain further traction.

VI. Conclusion

This paper presents a novel pneumatic-driven duplex-chambered inchworm mechanism for in-pipe robots. The mechanism is capable of bi-directional locomotion driven by only two air supply lines using pressure differences. We described the concept and structure of the mechanism and performed a theoretical analysis from the viewpoint of applied pressures. Various experiments were performed with a prototype to elucidate its characteristics, including elongation length and force generation, and the necessary pressure conditions to generate the locomotion pattern were discussed. In the final in-pipe locomotion test, the prototype achieved a locomotion speed of 45.5 mm/s in horizontal pipes; this is faster than previously reported pneumatic mechanisms of this size that move bi-directionally and can be improved even further. In the near future, we will examine and model the force generation characteristics of the mechanism to optimize the design. Additionally, we plan to improve the mechanism with features including a readily camera-attachable structure and steering mechanism.

References

[1] K. Suzumori *et al.*, "Micro inspection robot for 1-in pipes," *IEEE/ASME Trans. Mechatronics*, vol. 4, no. 3, pp. 286–292, 1999.

[2] E. Dertien *et al.*, "Development of an inspection robot for small diameter gas distribution mains," in *Proc. IEEE Int. Conf. Robot. Automat.*, 2011, pp. 5044–5049.

[3] E. Dertien *et al.*, "Design of a robot for in-pipe inspection using omnidirectional wheels and active stabilization," in *Proc. IEEE Int. Conf. Robot. Automat.*, 2014, pp. 5121–5126.

[4] E. Sachdeva *et al.*, "Design and optimal springs stiffness estimation of a modular OmniCrawler in-pipe climbing robot," in *Proc. IEEE Int. Conf. Robot. Biomim.*, 2017, pp. 1912–1917.

[5] P. Debenest *et al.*, "PipeTron series - Robots for pipe inspection," in *Proc. 3rd Int. Conf. Appl. Robot. Power Ind.*, 2014, pp. 1–6.

[6] J. Nagase *et al.*, "Development of Worm-Rack Driven Cylindrical Crawler Unit," *J. Adv. Mech. Design Syst. Manuf.*, vol. 7, no. 3, pp. 422–431, 2013.

[7] J. Nagase and F. Fukunaga, "Development of a novel crawler mechanism for pipe inspection," in *Proc. 42nd Annu. Conf. IEEE Ind. Electron. Soc.*, 2016, pp. 5873–5878.

[8] F. Fukunaga and J. Nagase, "Cylindrical elastic crawler mechanism for pipe inspection inspired by amoeba locomotion," in *Proc. 2016 6th IEEE Int. Conf. Biomed. Robot. Biomech.*, 2016, pp. 424–429.

[9] Y.-S. Kwon and B.-J. Yi, "Design and Motion Planning of a Two-Module Collaborative Indoor Pipeline Inspection Robot," *IEEE Trans. Robot.*, vol. 28, no. 3, pp. 681–696, 2012.

[10] S. Wakimoto *et al.*, "A micro snake-like robot for small pipe inspection," in *Proc. Int. Symp. Micromech. Human Sci.*, 2003, pp. 303–308.

[11] A. Brunete *et al.*, "A 2 DoF Servomotor-based Module for Pipe Inspection Modular Micro-robots," in *Proc. IEEE/RSJ Int. Conf. Intell. Robot.Syst.*, 2006, pp. 1329–1334.

[12] A. Kuwada *et al.*, "Snake-like robot negotiating three-dimensional pipelines," in *Proc. IEEE Int. Conf. Robot. Biomim.*, 2007, pp. 989–994.

[13] A. Kuwada *et al.*, "Automatic pipe negotiation control for snake-like robot," in *Proc. IEEE/ASME Int. Conf. Adv. Intell. Mech.*, 2008, pp. 558–563.

[14] M. Ikeuchi *et al.*, "Development of an in-pipe inspection robot for narrow pipes and elbows using pneumatic artificial muscles," in *Proc. IEEE/RSJ Int. Conf. Intell. Robot.Syst.*, 2012, pp. 926–931.

[15] Y. Tanise *et al.*, "High-speed response of the pneumatic actuator used in a peristaltic crawling robot inspecting long-distance gas pipes," in *Proc. IEEE Int. Conf. Adv. Intell. Mech.*, 2016, pp. 1234–1239.

[16] S. Yamazaki *et al.*, "Development of axial extension actuator for narrow pipe inspection endoscopic robot," in *Proc. IEEE/SICE Int. Symp. Syst. Integr.*, 2016, pp. 634–639.

[17] M. Kamata *et al.*, "Development of pneumatically driven peristaltic-type robot for long distance inspection in half-inch pipes," in *Proc. IEEE Int. Conf. Adv. Intell. Mech.*, 2017, pp. 309–314.

[18] H. Tsukagoshi *et al.*, "A Self-Propelled Catheter Capable of Generating Travelling Waves with Steering Function by Mono-Line Drive," in *Proc. IEEE Int. Conf. Robot. Automat.*, 2018, pp. 38–43.

[19] J. Qiao *et al.*, "Development of Inchworm In-Pipe Robot Based on Self-Locking Mechanism," *IEEE/ASME Trans. Mechatronics*, vol. 18, no. 2, pp. 799–806, 2013.

[20] A. A. Calderón *et al.*, "Design, fabrication and control of a multi-material-multi-actuator soft robot inspired by burrowing worms," in *Proc. IEEE Int. Conf. Robot. Biomim.*, 2016, pp. 31–38.

[21] H. Heung *et al.*, "Design and prototyping of a soft earthworm-like robot targeted for GI tract inspection," in *Proc. IEEE Int. Conf. Robot. Biomim.*, 2016, pp. 497–502.

[22] K. Nomura *et al.*, "Development of in-pipe robot with extension hose and balloons," in *Proc. IEEE Int. Conf. Mech. Automat.*, 2017, pp. 1481–1486.

[23] M. D. Gilbertson *et al.*, "Serially Actuated Locomotion for Soft Robots in Tube-Like Environments," *IEEE Robot. Autom. Lett.*, vol. 2, no. 2, pp. 1140–1147, 2017.

[24] K. Miyasaka *et al.*, "Long-mover: Flexible Tube In-pipe Inspection Robot for Long Distance and Complex Piping," in *Proc. IEEE/ASME Int. Conf. Adv. Intell. Mech.*, 2018, pp. 1075–1080.

[25] M. Kamata *et al.*, "Proposal of One-inch Pipe Inspection Robot "PI-RO I"," in *Proc. 7th IEEE Int. Conf. Biomed. Robot. Biomech.*, 2018, pp. 1315–1320.

[26] X. Zhang *et al.*, "A Biomimetic Soft Robot for Inspecting Pipeline with Significant Diameter Variation," in *Proc. IEEE/RSJ Int. Conf. Intell. Robot.Syst.*, 2018, pp. 7486–7491.

[27] Z. Zhang *et al.*, "Design and Modeling of a Parallel-Pipe-Crawling Pneumatic Soft Robot," *IEEE Access*, vol. 7, pp. 134 301–134 317, 2019.

[28] J. Lim *et al.*, "Pneumatic robot based on inchworm motion for small diameter pipe inspection," in *Proc. IEEE Int. Conf. Robot. Biomim.*, 2007, pp. 330–335.

[29] J. Lim *et al.*, "One pneumatic line based inchworm-like micro robot for half-inch pipe inspection," *Mechatronics*, vol. 18, no. 7, pp. 315–322, 2008.

[30] T. Takayama *et al.*, "A Twisted Bundled Tube Locomotive Device Proposed for In-Pipe Mobile Robot," *IEEE/ASME Trans. Mechatronics*, vol. 20, no. 6, pp. 2915–2923, 2015.

[31] H. Takeshima and T. Takayama, "Six-braided tube in-pipe locomotive device," in *Proc. IEEE/RSJ Int. Conf. Intell. Robot.Syst.*, 2015, pp. 1125–1130.

[32] T. Yamamoto *et al.*, "A high-speed locomotion mechanism using pneumatic hollow-shaft actuators for in-pipe robots," in *Proc. 2015 IEEE/RSJ Int. Conf. Intell. Robot.Syst.*, 2015, pp. 4724–4730.

[33] T. Yamamoto *et al.*, "A self-locking-type expansion mechanism to achieve high holding force and pipe-passing capability for a pneumatic in-pipe robot," in *Proc. IEEE Int. Conf. Robot. Automat.*, 2017, pp. 1900–1907.

[34] T. Yamamoto *et al.*, "High-speed sliding-inchworm motion mechanism with expansion-type pneumatic hollow-shaft actuators for in-pipe inspections," *Mechatronics*, vol. 56, pp. 101–114, 2018.

[35] K. Wakana *et al.*, "Pneumatic flexible hollow shaft actuator with high speed and long stroke motion," in *Proc. 2013 IEEE Int. Conf. Robot. Automat.*, 2013, pp. 357–363.